

Multifractal Analysis of Pulsar Timing Residuals: Assessment of Gravitational Waves Detection

I. Eghdami and H. Panahi*

Department of Physics, University of Guilan, Rasht 41635-1914, Iran

S. M. S. Movahed

Department of Physics, Shahid Beheshti University, Velenjak, Tehran 19839, Iran

(Dated: April 28, 2017)

Relying on multifractal behavior of pulsar timing residuals (*PTRs*), we examine the capability of Multifractal Detrended Fluctuation Analysis (MF-DFA) and Multifractal Detrending Moving Average Analysis (MF-DMA) modified by Singular Value Decomposition (SVD) and Adaptive Detrending (AD), to detect footprint of gravitational waves (GWs) superimposed on *PTRs*. Mentioned methods enable us to clarify the type of GWs which is related to the value of Hurst exponent. We introduce three strategies based on generalized Hurst exponent and width of singularity spectrum, to determine the dimensionless amplitude of GWs. For a stochastic gravitational wave background with characteristic strain spectrum as $\mathcal{H}_c(f) \sim \mathcal{A}f^\zeta$, the dimensionless amplitude greater than $\mathcal{A} \gtrsim 10^{-17}$ can be recognized irrespective to value of ζ . We also utilize MF-DFA and MF-DMA to explore 20 millisecond pulsars observed by Parkes Pulsar Timing Array (PPTA). Our analysis demonstrates that there exists a cross-over in fluctuation function versus time scale for observed timing residuals representing a universal property and equates to $s_\times \sim 60$ days. To assess multifractal nature of observed timing residuals, we apply AD and SVD algorithms on time series as pre-processes to remove superimposed trends as much as possible. The scaling exponents determined by MF-DFA and MF-DMA confirm that, all data are classified in non-stationary class elucidating second universality feature. The value of corresponding Hurst exponent is in interval $H \in [0.35, 0.85]$. The q -dependency of generalized Hurst exponent demonstrates observed *PTRs* have multifractal behavior and the source of this multifractality is mainly devoted to correlation of data which is another universality of observed data sets.

PACS numbers:

I. INTRODUCTION

Pulsar timing has received extensive attention due to regularity rotation of pulsar for astrophysical interests [1, 2]. A relevant observable devoted to a pulsar is so-called pulsar timing residual defined by difference between the measured time of arrival (TOA) and those anticipated by a timing model [1]. Observed pulsar timing residual (*PTR*) is a good indicator to elucidate some interesting physical properties of pulsar as well as other cosmological and astrophysical foreground phenomena affecting on that [3]. Due to unknown physical phenomena govern on the variation of pulsar's spin and spin-down as well as foreground effects, *PTR* can be categorized in $1+1$ dimensional stochastic process (one of parameters is independent parameter while the other parameter is represented as a function of independent parameter). This stochasticity enforces to apply robust methods to extract reliable information for further analysis.

Millisecond pulsars (MSPs) were first suggested as detectors of gravitational waves (GWs) by Sazhin (1978) [4] and Detweiler (1979) [5] because of high stability and predictability of their rotational behavior (see also [6]). Indeed, GWs can be produced according to different mechanisms ranging from early epoch to present era. Continuous wave sources [7], burst sources [8–10] and stochastic backgrounds [11, 12] are most well-known classifications of GWs. As an illustration, one can point out to relic GWs including GWs by cosmic strings and primordial perturbations [12–15]. Other important sources for GWs are known as formation of supermassive black holes and binary black hole mergers [16, 17]. Recently, the GWs of black hole mergers has been recorded by LIGO detectors which can be an evidence of dark matter in the early universe or corresponds to the binary black hole of stellar origin [18]. An other classification of GWs is devoted to continuous, inspiral, burst and stochastic types of GWs [19, 20]. In order to detect mentioned types of GWs, many approaches have been proposed and utilized during past decades [20–23]. Very low amplitude of GWs, different sources and mechanisms for GWs production, in one hand and in other hand, the extended range of frequency lead to introduce various indirect approaches such as predictions of energy loss because of gravitational wave emission [24] and direct approaches such as detecting the effect of gravitational waves on pulsar timing residuals [23]. So, two main methods for detection of GWs are known as interferometers (such as LISA and LIGO) and pulsar timing arrays [25].

For frequency interval $\nu \in [10^{-8} - 10^{-6}]$, there are several pulsar timing array projects devoted to observe the imprint of GWs using pulsar timing detectors [26].

* Corresponding author email: t-panahi@guilan.ac.ir

In the context of pulsar timing array approach, some famous projects have been proposed, namely the Parkes Pulsar Timing Array (PPTA) [3, 27, 28], the European Pulsar Timing Array (EPTA) [29, 30], the North American Nanohertz Observatory for Gravitational Waves (NANOGrav) [31, 32] and International Pulsar Timing Array (IPTA) [1]. Beside mentioned projects, the Square Kilometer Array (SKA) [33, 34] radio telescope would further improve the sensitivity of pulsar timing measurements to detect GWs.

More recently, Zhu et al., introduced coherent method for observing and determining sky localization of continuous GWs from non-evolving binaries with pulsar timing array [35, 36]. One can refer to [37–39], for a complementary discussion on various experiments and methods to detect GWs.

Pulsar Timing Array utilizing the Parkes radio telescope in Australia is an attempt to detect GWs by observing 20 bright MSPs [3]. This goal needs to a high precision of observation and according to the results of Ref. [23] the PPTA observations must be continue more than five years in order to achieve a precision of 100 ns.

Since pulsar timing residuals are induced by GWs [23], therefore some authors used the statistical correlation of pulsars timing residuals to evaluate their capability to detect GWs [23, 40].

If we want to use *PTRs* data sets to elaborate the benchmark of different types of GWs, two following aspect should be considered: first of all, relying on various sources of GWs encourage us to find deep insight regarding the properties of GWs emitted by different sources. The second aspect is that, we should examine the performance of different statistical methods and their sensitivities. Those methods which are capable to satisfy relevant conditions, are categorized in robust analysis group. As mentioned before, a typical GW can be produced by a single or a population of supermassive binary black holes. GWs produced by single sources have weak anisotropic distribution and the weakness of this case leads to abolish the performance of two point correlation function for discriminations between different sources [25].

In addition, due to complexity nature of pulsar data sets as well as the presence of foreground and systematic noises, consequently, underlying data are mimicked by trends and noises. Subsequently, it is necessary to implement robust and novel methods for removing destructive effects from desired part of signals. Such case motivates us to look for more sensitive methods for analyzing pulsar timing residuals in the presence of noises and various trends.

What we have done in this paper has following advantages and novelties: Inspired by properties of a self-similar process characterized by a scaling exponent which is so-called "Hurst exponent" [41–44], for the first time, we have used Multifractal Detrended Fluctuations (MF-DFA) [45, 46] and Multi-Fractal Detrended Moving Average Analysis (MF-DMA) [47, 48] methods on the observed (including 20 MSPs inferred from [3]) and sim-

ulated pulsar timing residuals as well as GWs signals (TEMPO2 software package [49]), in order to evaluate the multiscaling behavior of underlying data from statistical point of view. We modify MF-DFA and MF-DMA by additional detrending algorithms, namely Adaptive Detrending (AD) [50] and Singular Value Decomposition (SVD) [51–53] methods to exclude or at least decrease the contribution of unknown trends and noises as much as possible. These methods are utilized as pre-complementary detrending procedure. We check whether pulsar timing residuals are multifractal or not and in the case of multifractality, we determine the sources of multifractality based on statistical approach. Also this research demonstrates that, there exist criteria not only for discrimination of the footprint of stochastic GWs background and single sources GWs on pulsar timing residual but also for determining the corresponding dimensionless amplitude. Finally, this view provides a new insight to utilize pulsar timing residuals for further astrophysical usages.

The rest of this paper is organized as follows: In section II, we will explain MF-DFA, MF-DMA, Adaptive detrending and SVD in details. Section III is devoted to theoretical notions of gravitational wave background and data description for observed as well as synthetic data sets. We will implement the multifractal methods on simulated and observed timing residuals series in section IV. The capability of detecting GWs in the sensitive range of pulsar timing residual series, will be discussed in this section. Three strategies to reveal the imprint of GWs on the residual time series in a noiseless observation will be explained. We will assess the multifractality of observed pulsar timing residuals in mentioned section. Section V is bequeathed to summary and conclusion.

II. METHODOLOGY: MULTIFRACTAL ANALYSIS

Non-stationary sources including trends and artificial noises usually influence the observed time series. In order to inference reliable results, mentioned spurious effects should be well characterized from the intrinsic fluctuations. Concerning trends, in the literatures, Z. Wu et al., [54] stated that, in principle there is no universal definition for trend and any proper algorithm for evoking from underlying series. One of the well-studied methods for this purpose is Multifractal Detrended Fluctuations Analysis (MF-DFA) [45, 46] applied to various areas, ranging from economical time series [55–58], river flow [59] and sunspot fluctuations [50, 60], cosmic microwave background radiations [61], music [62, 63], plasma fluctuations [64], traffic jamming [65], image processing and medical measurements [66, 67], to astronomy [68]. Cross-correlation has been also introduced and applied in some cases [69–74] and its generalized, the Multifractal Detrended Cross-Correlation Analysis (MF-DXA) examining higher orders detrended covariance [75]. Although

the approach in multifractal detrended analysis such as MF-DFA and MF-DXA methods diminishes polynomial trends but previous researches demonstrated that sinusoidal and power-law trends are not completely removed [76, 77]. In order to eliminate above trends, there are several robust methods have been proposed: Fourier Detrended Fluctuations Analysis (F-DFA) [78, 79], Singular Value Decomposition (SVD) [51–53], Adaptive Detrending method (AD) [50], and Empirical mode decomposition (EMD)[80]. In this paper we will use MF-DFA, MF-DMA. In order to remove cross-over in our results we also carry out AD and SVD approaches for further cleaning pre-processes. In this section we introduce the main algorithms for applying MF-DFA, MF-DMA, AD and SVD methods.

A. MF-DFA

The multifractal detrended fluctuation analysis is a modified version of detrended fluctuation analysis. The main steps for this method are as follows: [46, 50, 81–84]

(1) : We call the pulsar timing residual (*PTR*) as input data set for examining multifractal property as:

$$PTR(i), \quad i = 1, \dots, N. \quad (1)$$

(2) : To magnify the hidden self-similarity property, we make profile series, accordingly by integrating the original series $\{PTR\}$ as:

$$X(j) = \sum_{i=1}^j [PTR(i) - \langle PTR \rangle] \quad , \quad j = 1, \dots, N. \quad (2)$$

(3) : To extract embedded trends in underlying data set, according to DFA method, the profile series $\{X\}$ should be divided into $N_s = \text{int}(N/s)$ non-overlapping segments of length s . The range of non-overlapping windows value is $N_s \in [N_s^{\min}, N_s^{\max}]$. In order to take into account the remaining unused part of data from the opposite end of data, the enumeration must to be repeated from the mentioned part. In this case we will have $2N_s$ segments. In this task, one should compute fluctuation function in each produced segments as follows:

$$\mathcal{F}^2(s, \nu) = \frac{1}{s} \sum_{i=1}^s \left[X(i + (\nu - 1)s) - \tilde{X}_\nu(i) \right]^2, \quad (3)$$

for segments $\nu = 1, \dots, N_s$ and for opposite end we have:

$$\mathcal{F}^2(s, \nu) = \frac{1}{s} \sum_{i=1}^s \left[X(i + N - (\nu - N_s)s) - \tilde{X}_\nu(i) \right]^2, \quad (4)$$

for segments $\nu = N_s + 1, \dots, 2N_s$. Here, $\tilde{X}_\nu(i)$ is a fitting polynomial function in the ν -th segment with arbitrary order describing the local trend. Usually a linear function for modeling local trend is considered while if there is no superimposed trend on fluctuation, then a zeroth

order fitting function is expected to be enough [85]. It must point out that MF-DFA m denotes that the order of polynomial function used in MF-DFA is " m ". Throughout this paper we take $m = 1$ unless mentioned otherwise. According to previous researches, the minimum value of data in each segments may impose some uncertainty in determining scaling properties. By construction, the fluctuations function is defined for $s > m + 2$ [46]. On the other hand, this method becomes unreliable for very large windows size ($s > \frac{N}{4}$).

(4) : To examine multifractality nature the q -th order fluctuation function by averaging over all segments should be computed as:

$$\mathcal{F}_q(s) = \left(\frac{1}{2N_s} \sum_{\nu=1}^{2N_s} [\mathcal{F}^2(s, \nu)]^{q/2} \right)^{1/q}, \quad (5)$$

the q -parameter can take any real value except zero. Using L' Hôpital's rule for $q = 0$ we find:

$$\mathcal{F}_0(s) = \exp \left(\frac{1}{4N_s} \sum_{n=1}^{2N_s} \ln \mathcal{F}^2(s, n) \right). \quad (6)$$

Various values of the parameter q enable us to quantify the contribution of different values of fluctuation functions in Eqs. (5) and (6). Consequently, for negative values of q , small fluctuations have dominant contribution in summation, on the contrary, positive values of q cause the larger value of fluctuation contributions. For $q = 2$ the common DFA is retrieved.

(5) : The scaling behavior of the fluctuation function $\mathcal{F}_q(s)$ by considering the scaling relation as:

$$\mathcal{F}_q(s) \sim s^{h(q)}. \quad (7)$$

Any q -dependency of $h(q)$, represents that underlying data set is multifractal. The scaling exponent $h(q)$ is called the generalized Hurst exponent. For class of non-stationary series (corresponds to fractional Brownian motion (fBm)) exponent derived by MF-DFA is $h(q = 2) > 1$, therefore in this case Hurst exponent is given by: $H = h(q = 2) - 1$. In stationary case $h(q = 2) < 1$ (corresponds to fractional Gaussian noise (fGn)). For completely stationary random data $H = 0.5$, while for persistent data set $0.5 < H < 1.0$. For anti-correlated data set, $H < 0.5$ [82, 86, 87]. Whenever Hurst exponent is determined, the scaling exponents of auto-correlation ($C(\tau)$) and power spectrum ($S(f)$) can be given according to their analytic relations to Hurst exponent. We summarize these relations in Tab. I.

Standard multifractal formalism demonstrates the following relation between generalized Hurst exponent and the scaling exponent of partition function of underlying series which is so-called multifractal scaling exponent as follows [46]:

$$\xi(q) = qh(q) - 1. \quad (8)$$

Exponent	1D-fGn	1D-fBm
Exponent to correlation function (γ) $C(\tau) \sim \tau^{-\gamma}$	$2 - 2H$	$-2H$
Exponent for power spectrum (β) $S(f) \sim f^{-\beta}$	$2H - 1$	$2H + 1$

TABLE I: Some relevant exponents related to stochastic processes in 1 + 1 dimension.

For monofractal data set, $\xi(q)$ is a linear function [46]. The generalized multifractal dimension is also given by:

$$D(q) = \frac{\xi(q)}{q-1} = \frac{qh(q)-1}{q-1}, \quad (9)$$

where $D(q=0) = D_f$ is the fractal dimension of time series and $D(q=1)$ is related to the so-called entropy of underlying system [88]. To make more complete quantitative measure for multifractality, the so-called singularity spectrum indicating how the box probability of standard multifractal formalism behaves at small scales, is defined by Legendre transformation of $\xi(q)$ as [89]:

$$f(\alpha) = \alpha q - \xi(q), \quad (10)$$

and the Hölder exponent is $\alpha \equiv d\xi(q)/dq$. In the case of multifractality, a spectrum of Hölder exponent is appeared instead of having single exponent. The domain of Hölder spectrum, $\alpha \in [\alpha_{\min}, \alpha_{\max}]$, becomes [90, 91]:

$$\alpha_{\min} = \lim_{q \rightarrow +\infty} \frac{\partial \xi(q)}{\partial q}, \quad (11)$$

$$\alpha_{\max} = \lim_{q \rightarrow -\infty} \frac{\partial \xi(q)}{\partial q}. \quad (12)$$

Subsequently, the width $\Delta\alpha \equiv \alpha_{\max} - \alpha_{\min}$ is a reliable measure for quantifying multifractality nature of underlying data. The higher value of $\Delta\alpha$ the higher multifractality nature which is a benchmark for complexity of underlying signal.

B. MF-DMA

Since, in MF-DFA, there is a discontinuity for fitting a polynomial at the boundary of each partition, MF-DMA has been introduced to decrease this artifact for determining generalized Hurst exponent [47, 48]. The corresponding algorithm is explained as follows:

(1) : For a typical pulsar timing residual series with length of N , we should create a cumulative time series as follows:

$$X(j) = \sum_{i=1}^j [PTR(i) - \langle PTR \rangle], \quad j = 1, \dots, N. \quad (13)$$

here the removing of mean value is not compulsory because detrending in each moving window will be done in

order to remove any local and almost global effect depending on window's size.

(2) : For each moving window with size s , we calculate the moving average function:

$$\widetilde{X}(j) = \frac{1}{s} \sum_{k=-s_1}^{s_2} X(j-k), \quad (14)$$

where $s_1 = \lfloor (s-1)\theta \rfloor$ and $s_2 = \lceil (s-1)(1-\theta) \rceil$. The symbol $\lfloor a \rfloor$ represents the largest integer value not greater than a and $\lceil a \rceil$ is devoted to the smallest integer value not smaller than a . In above equation θ plays a crucial role. For $\theta = 0$, mentioned approach refers to backward moving average while $\theta = 1$ is so-called forward moving average and finally $\theta = 0.5$ refers to the centered moving average [47, 92].

(3) : Detrended data is constructed by subtracting calculated moving average function from the cumulative series X as:

$$\varepsilon(i) = X(i) - \widetilde{X}(i), \quad (15)$$

where $s - s_1 \leq i \leq N - s_1$

(4) : Now $\varepsilon(i)$ is divided into $N_s = \text{int}[N/s]$ non-overlapping windows with the same size of s and we calculate the fluctuation function:

$$\mathcal{F}^2(s, \nu) = \frac{1}{s} \sum_{i=1}^s \varepsilon^2(i + (\nu-1)s). \quad (16)$$

(5) : For multifractal analysis, the q th order of overall fluctuation function is obtained by:

$$\mathcal{F}_q(s) = \left(\frac{1}{N_s} \sum_{\nu=1}^{N_s} [\mathcal{F}^2(s, \nu)]^{q/2} \right)^{\frac{1}{q}}, \quad (17)$$

for $q = 0$ according to L'Hôpital's rule, we have:

$$\mathcal{F}_0(s) = \exp \left(\frac{1}{2N_s} \sum_{\nu=1}^{N_s} \ln \mathcal{F}^2(s, \nu) \right). \quad (18)$$

Finally, the fluctuation function $\mathcal{F}_q(s)$ is supposed to have the following scaling form:

$$\mathcal{F}_q(s) \sim s^{h(q)}. \quad (19)$$

The rest scaling exponents and singularity spectrum $f(\alpha)$ can be evaluated same as Eqs.(8)-(12) for a multifractal analysis.

C. Singular Value Decomposition (SVD)

It is important to find and eliminate trends in data analysis specially in astronomical data. When we use MF-DFA or MF-DMA, an essential demand corresponding to present a scaling behavior must be satisfied as stated in Eqs. (7) and (19). In some cases, there exist one or more

crossover which corresponds to different correlation behavior of pattern in various scales [52, 53, 76, 77, 79, 93]. Different reasons can make these crossovers. Since the MF-DFA and MF-DMA methods can not remove the effect of all trends, we implement complementary tasks in order to manage the scaling behavior of fluctuation functions properly and to obtain the reliable fluctuation exponent and generalized Hurst exponent. There are some pre-processings for removing trends in the literatures for instance empirical mode decomposition (EMD) method [80], Fourier-Detrended (Fourier-based filtering) method [78, 79], Singular Value Decomposition (SVD) method [51–53] and Adaptive Detrending (AD) algorithm [50]. In this paper to extract trends, we utilize SVD method and Adaptive detrending algorithm. By employing the SVD method, we can track the influence of sinusoidal trend types on the results. In addition, the size of output data preserves in this method [52, 53]. In addition, it enables to find out the scale of domination of trends or noises.

The main part of SVD method can be described in the following steps [52, 53, 94]:

(I): Pulsar timing residual data sets represented by $\{PTR(i)\}; i = 1, \dots, N$ might be superimposed with some periodic trends. We construct a matrix which its elements are pulsar timing residual with following order:

$$\mathbf{\Gamma} \equiv \begin{pmatrix} PTR_1 & PTR_{1+\tau} & \dots & PTR_{1+N-(d-1)\tau-1} \\ \vdots & \vdots & \vdots & \vdots \\ PTR_i & PTR_{i+\tau} & \dots & PTR_{i+N-(d-1)\tau-1} \\ \vdots & \vdots & \vdots & \vdots \\ PTR_d & PTR_{d+\tau} & \dots & PTR_{d+N-(d-1)\tau-1} \end{pmatrix}, \quad (20)$$

where d is embedding dimension and τ is the time delay. Also we have $1 \leq i \leq d$. Considering a time series of size N , the maximum value of embedding dimension d is equal to $d \leq N - (d-1)\tau + 1$ [53, 79, 95]. (II): Decomposing matrix $\mathbf{\Gamma}$ to left ($\mathbf{U}_{d \times d}$) and right ($\mathbf{V}_{(N-(d-1)\tau) \times (N-(d-1)\tau)}$) orthogonal matrices:

$$\mathbf{\Gamma} = \mathbf{U}\mathbf{S}\mathbf{V}^\dagger, \quad (21)$$

where $\mathbf{S}_{d \times (N-(d-1)\tau)}$ is a diagonal matrix and its elements are the desired singular values. For a trend containing p dominant frequencies, we set $2p + 1$ eigenvalues of matrix \mathbf{S} to zero for eliminating long periods on the contrary, to diminish short period fluctuations, we keep some dominant eigenvalues and we set the $d - p$ eigenvalues to zero. In other word, p dominant eigenvalues and associated eigenvectors correspond to long wavelengths subspace while $d - p$ eigenvalues and corresponding eigendecomposed vectors represent short wavelengths subspace. Finally, the new eigenvalues matrix which is called $\tilde{\mathbf{S}}$ is determined for further analysis. Then according to filtered matrix $\tilde{\mathbf{\Gamma}} = \mathbf{U}\tilde{\mathbf{S}}\mathbf{V}^\dagger$, the filtered time series is constructed as:

$$\widetilde{PTR}_{i+j-1} = \tilde{\Gamma}_{ij}, \quad (22)$$

here $1 \leq i \leq d$ and $1 \leq j \leq N - (d-1)\tau$. Now the cleaned \widetilde{PTR} data sets will be used as input for MF-DFA or MF-DMA discussed in previous subsections.

D. Adaptive Detrending method

As mentioned before, a robust algorithm to resolve discrepancy regarding the presence of trend is the adaptive detrended method introduced in [50]. The implementation of adaptive detrending algorithm is a complementary method for determining local and global trends. Therefore, after applying adaptive detrending method on observed pulsar timing series, the corresponding output data will be used as an input for MF-DFA or MF-DMA methods explained before. Adaptive detrending includes following steps [50]:

(1) Discrete series, $PTR(i)$ with $i = 1, \dots, N$ is partitioned with overlapping windows of length $2n + 1$ and accordingly, each neighboring segment has $n + 1$ overlapping points. An arbitrary polynomial \mathcal{Y} is constructed in each window of length $2n + 1$. In order to have continuous trend function avoiding a typical sharp jump in it, the following weighted function for the overlapping part of the ν th segment is considered [50]:

$$\mathcal{Y}_\nu^{\text{overlap}}(j) = \left(1 - \frac{j-1}{n}\right) \mathcal{Y}_\nu(j+n) + \frac{j-1}{n} \mathcal{Y}_{\nu+1}(j),$$

where $j = 1, 2, \dots, n + 1$. The two free parameters namely n and the order of the fitting polynomial should be determined properly [50]. The size of each segment was calculated by, $2n + 1 = 2\text{int}[(N-1)/(w_{\text{adaptive}} + 1)] + 1$. It turns out that by increasing the value of w_{adaptive} and the order of the fitting polynomial, basically the fluctuations disappear and, consequently, the fluctuations are suppressed. For the non-overlapping segments the adaptive detrended data is given by $\widetilde{PTR}(i) = PTR(j) - \mathcal{Y}_\nu(i)$, while for the overlap part is, $\widetilde{PTR}(i) = PTR(j) - \mathcal{Y}_\nu^{\text{overlap}}(i)$. Now, $\widetilde{PTR}(i)$ is used for further analysis in MF-DFA or MF-DMA.

E. Posterior Analysis

An approach to determine the reliable value of generalized Hurst exponent (Eqs. (7) and (19)), is Bayesian statistics [96]. Suppose that measurements and model parameters are indicated as $\{\mathcal{D}\} : \{\mathcal{F}_q(s)\}$ and $\{\Theta\} : \{h(q)\}$, respectively. In this approach the posterior function is:

$$\mathcal{P}(h(q)|\mathcal{D}) = \frac{\mathcal{L}(\mathcal{D}|h(q))\mathcal{P}(h(q))}{\int \mathcal{L}(\mathcal{D}|h(q))dh(q)}, \quad (23)$$

here \mathcal{L} is Likelihood and $\mathcal{P}(h(q))$ is prior probability function including all initial constraints concerning model parameters. Finally the χ^2 for determining the best fit

value for scaling exponent coordinated by multifractal formalism reads as:

$$\chi^2(h(q)) \equiv \Delta^\dagger \mathcal{C}^{-1} \Delta, \quad (24)$$

where $\Delta \equiv [\mathcal{F}_q^{\text{obs.}} - \mathcal{F}_q^{\text{the.}}]$ and \mathcal{C} is the covariance matrix. In addition $\mathcal{F}_q^{\text{obs.}}(s)$ and $\mathcal{F}_q^{\text{the.}}(s; h(q))$ are fluctuation functions computed directly from the and determined by Eqs. (7) or (19), respectively. According to following integral, the value of error-bar at 1σ confidence interval of $h(q)$ is determined by:

$$68.3\% = \int_{-\sigma_h^-}^{+\sigma_h^+} \mathcal{L}(\mathcal{D}|h(q)) dh(q). \quad (25)$$

Subsequently, we report the best value of scaling exponent at 1σ confidence interval according to $h(q)_{-\sigma_h^-}^{+\sigma_h^+}$.

In the following sections we will explain theoretical necessities for GWs and PTR s from observations and simulations.

III. DATA DESCRIPTION

In this section we will describe theoretical models for GWs signals from various sources. The observational data sets, synthetic series for pure timing residuals and GWs in order to examine multiscaling behavior of PTR as indicator of GWs, will be described in this section.

A. Theoretical notions of GWB on PTR

As discussed in various literatures, potential sources of GWs could be massive accelerated objects [16, 17], burst sources [8, 9] and stochastic background sources [12–15]. The latter candidate is almost supposed to be isotropic [6]. Isotropic stochastic gravitational wave background (GWB) produced by coalescing supermassive binary black holes mergers is the strongest potentially detectable signal of GWs [6], which we have used in our simulation. From theoretical point of view, one of general forms of characteristic strain spectrum, $\mathcal{H}_c(f)$, for a stochastic gravitational wave background can be described by following power law relation [13]:

$$\mathcal{H}_c(f) = \mathcal{A} \left(\frac{f}{f_{1yr}} \right)^\zeta, \quad (26)$$

where f is the frequency of GWs, $f_{1yr} = \frac{1}{1yr}$, \mathcal{A} is the dimensionless amplitude of GWBs and ζ is a scaling exponent and for almost all expected GWs is $\zeta < 0$. The corresponding ζ exponent takes following values for different mechanisms: $\zeta = -\frac{2}{3}$ for coalescing black hole binaries, $\zeta = -1$ for cosmic strings and $\zeta = -\frac{7}{6}$ for primordial GWs from Big-Bang [13]. Another framework for modeling strain spectrum, accounting the discrete nature

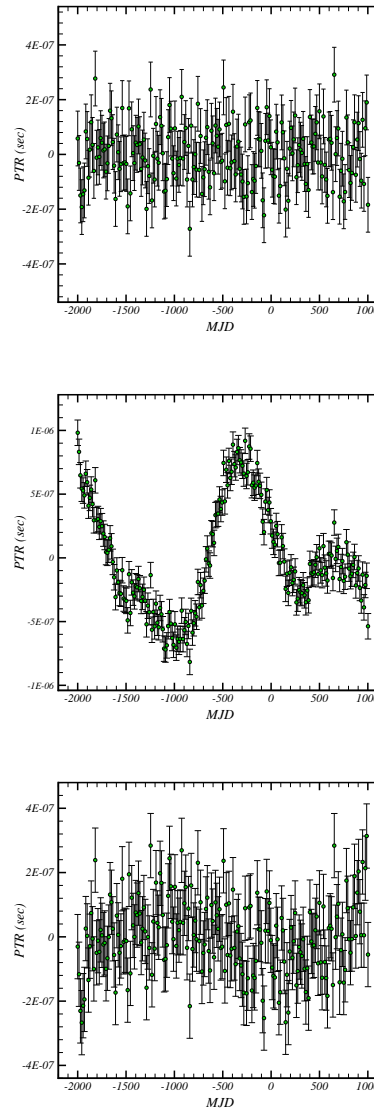


FIG. 1: Upper panel corresponds to a pure simulated timing residual. Middle panel shows a synthetic pure timing residual induced by GWB with dimensionless amplitude of $\mathcal{A} = 10^{-14}$. Lower panel illustrates the same as middle panel, just for $\mathcal{A} = 10^{-15}$. Here we take $\zeta = -2/3$.

of supermassive black holes for GWB leads so different functional form [97, 98]. The dimensionless amplitude of GWs has been predicted by most authors in range of $\mathcal{A} \in [10^{-15}, 10^{-14}]$ however according to Refs. [97, 98] the range of \mathcal{A} for a stochastic GWB is $\mathcal{A} \in [10^{-16}, 3 \times 10^{-15}]$.

B. Synthetic Data sets for GWB

To simulate synthetic series, we use TEMPO2 software package which is carrying out the fitting procedure of TOA [49]. In addition, this package can be used to simulate pure timing residuals [6]. To simulate GWB "GWbkgrd", plugin of TEMPO2 will be used [99]. Since the purpose of this paper is devoted to analyzing PTR data sets induced by GWs signals, therefore, we call PTR without any GWs signals by PTR_{pure} and when this series is modified by GWs fluctuations, we will have:

$$PTR(t) \equiv PTR_{\text{pure}}(t) + R(t), \quad (27)$$

here $R(t)$ corresponds to GWs signal and it is given by [6]:

$$R(t) = -\frac{1}{2} \text{Re} \left[\sum_j i \frac{\hat{k}_p^l \hat{k}_p^m A_{lm}^j}{\omega_j} (e^{-i\omega_j t} - 1) \times \left(\frac{1 - e^{i\omega_j D(1 - \cos \eta_j)}}{1 - \cos \eta_j} \right) \right], \quad (28)$$

where \hat{k}_p^l , η_j and ω_j are photon four-vector in the unperturbed space-time, angle between direction of the pulsar and direction of the GW source, and the angular frequency of the j th GW respectively. In addition, $D \equiv x_r^\mu - x_e^\mu$ is the travel time of photons between location of emitter (x_e^μ) and location of receiver (x_r^μ). The amplitude tensor A_{lm} is

$$A_{lm} = \begin{pmatrix} 0 & 0 & 0 \\ 0 & \mathcal{A}_+ & \mathcal{A}_\times \\ 0 & \mathcal{A}_\times & \mathcal{A}_+ \end{pmatrix}, \quad (29)$$

which \mathcal{A}_+ and \mathcal{A}_\times refer to two independent degree of freedom in Einstein equation. In order to test the effect of GWs on PTR s, according to Eq. (27), initially we simulate 100 pure timing residuals ($PTR_{\text{pure}}(t)$) for a single pulsar with a rms of 100 ns. This accuracy is about one order of magnitude greater than observed data released by PPTA [3] up to now (see Table II). Fig. 1 indicates a typical pure timing residual simulated by TEMPO2 with zero mean uncorrelated series. We depict superposition of perfect timing residuals with GWs modeled by Eq. (28), in Fig. 1. Finally, $PTR(t)$ will be considered as input series for multifractal analysis.

C. Observed Data

Since MSPs have stable rotating behavior and pulse emission, their timing residuals can be used to detect GWs and in this work we use timing residual data of 20 MSPs observed by PPTA project [3].

PPTA is a collaboration between Swinburne University of Technology, Commonwealth Scientific and Industrial Research Organization (CSIRO) Astronomy and Space

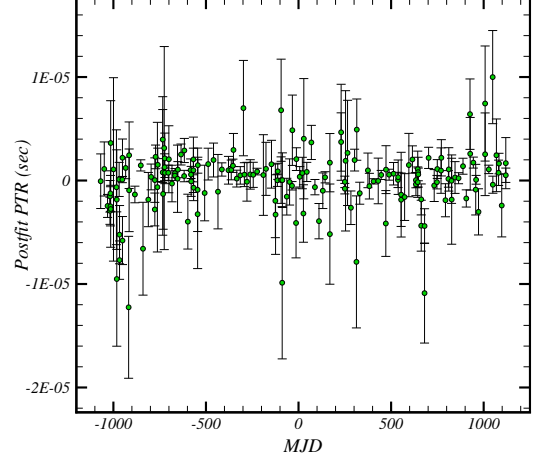


FIG. 2: Observed pulsar timing residual of PSR J1024-0719 by PPTA project.

Science Division (CASS) by implementing the Parkes 64-m radio telescope (PTA). The PTA telescope is located in Australia at altitude of -33° and can observe the whole of inner Galaxy. In this project 20 MSPs have been observed at three bandwidths namely 10cm, 20cm and 50cm. These 20 pulsars have been chosen by satisfying some criteria. Due to more stability of short period MSPs, observed pulsars have short periods selected from bright ones. Also these MSPs have narrow pulses width in order to reduce uncertainties in corresponding TOA. Finally, isolated either wide-binary MSPs have been selected to avoid the effects of companion star.

In this paper we take PTR series for mentioned MSPs as observed data sets are publicly available from [100]. The name of 20 MSPs with corresponding rms and total time span have been reported in Tab. II. It is worth noting that, several phenomena such as atmospheric delays, vacuum retardation due to observatory motion, Einstein delay and Shapiro delay can effect on the TOA [101] and they should be dismissed to have a post-fitted timing residual which is called PTR . Fig. 2 illustrates a typical post-fit pulsar timing residual of PSR J1024-0719 observed by PPTA project [3, 100]. The fitting procedure has been done by TEMPO2 software.

IV. IMPLEMENTATION OF MULTIFRACTAL METHODS ON PTR S

In this section we will use MF-DFA and MF-DMA accompanying AD and SVD methods separately, in order to evaluate the multifractal nature of synthetic data and the capability of our analysis as a detector of gravitational waves in simulation. We will provide a pipe-line for determining the type of GWB. After that, we apply our methods to examine the complexity of pulsar timing

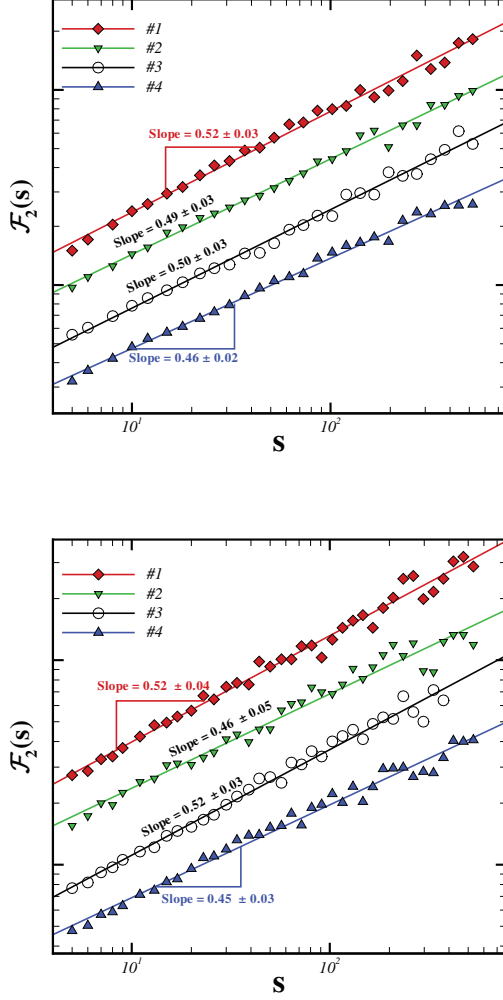


FIG. 3: Upper panel: Log-log plot of $\mathcal{F}_2(s)$ versus s computed by DFA for various simulated pure PTR s. While the lower panel corresponds to same as upper panel computed by DMA with $\theta = 0.0$. To make more sense, we shifted \mathcal{F}_2 vertically for different series. As we expect, the value of Hurst exponent for all data sets is consistent with completely random series.

residuals for clarifying the statistical behavior of observed pulsars.

A. Multifractal nature of synthetic Data

In this subsection, we turn to examine the multifractal nature of synthetic PTR (PTR_{pure}) and its superposition with simulated GWBs to show the capability of PTR s based on multifractal modeling in detecting GWs. At first, we rely on the statistical properties of $PTR_{\text{pure}}(t)$ in various simulations. Application of DFA and DMA on $PTR_{\text{pure}}(t)$ are indicated in Fig. 3. The value of Hurst

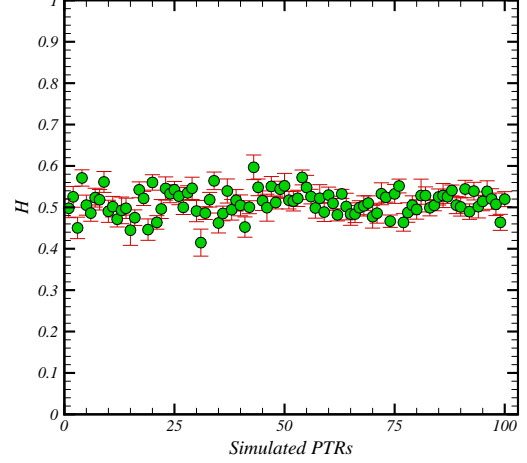


FIG. 4: Hurst exponent for 100 pure PTR s simulated by TEMPO2.

exponent for all PTR_{pure} simulated is indicated in Fig. 4. The average value is $\langle H \rangle = 0.51 \pm 0.02$ at 1σ level of confidence confirming that PTR_{pure} is uncorrelated data set [13].

Now we simulate GWB for a given set of initial parameters and superimpose them to pure PTR s according to Eq. (27). Before applying AD and SVD algorithms to make clean data sets, we apply DFA and DMA on simulated $PTR(t)$ for various amplitudes. Fig. 5 illustrates $\mathcal{F}_2(s)$ as a function of s for simulated series. These results confirm that there is a crossover in fluctuation functions versus s . The position of crossovers before applying SVD or AD methods depends on \mathcal{A} . For determining the value of Hurst exponent we apply SVD or AD and then clean series are used for further analysis by DFA and DMA methods. In Fig. 5, fluctuation functions given by DFA and DMA before and after applying SVD or AD methods have been shown. In the next subsection we will show that the slope of fluctuations function is also amplitude-dependent. We set $\theta = 0.0$ for DMA corresponding to backward DMA because, it has been demonstrated that backward DMA has the best performance [47]. Now, it is possible to assign scaling exponent for fluctuation function versus s . The generalized Hurst exponent and ξ versus q for three type of PTR s superimposed by different values of GWB amplitudes is plotted in Fig. 6. The lower plot in Fig. 6 illustrates singularity spectrum.

According to previous results for synthetic PTR s, we encourage to compare the multifractal nature of simulated PTR s induced by GWB signal, in order to examine the capability of this approach not only to detect the footprint of GWs but also to determine the amplitude of GWs.

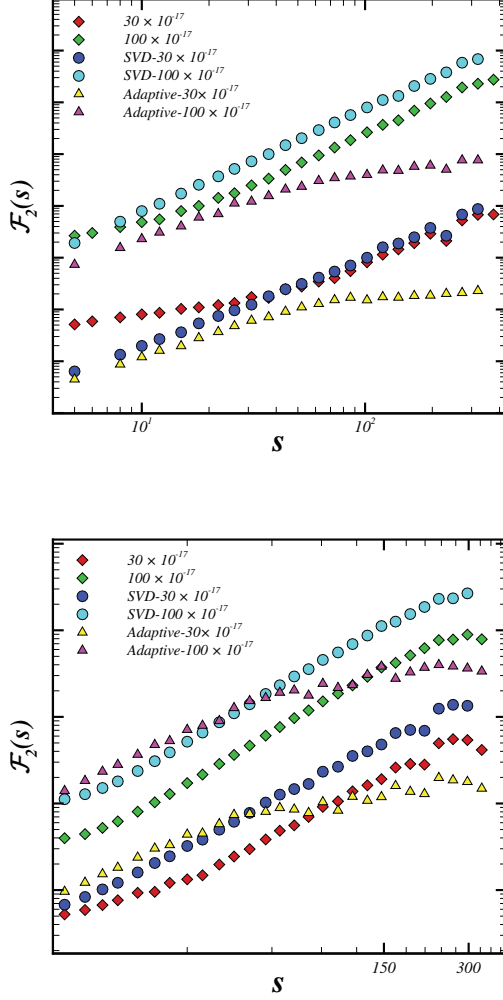


FIG. 5: Upper panel: Log-log plot of $\mathcal{F}_2(s)$ versus s computed by DFA for various simulated PTR s affected by stochastic GWs when we apply adaptive and SVD as pre-processes. While the lower panel corresponds to same as upper panel computed by DMA with $\theta = 0.0$.

To make more sense, we shifted \mathcal{F}_2 vertically for different simulations. In this figure we take $\zeta = -2/3$. Different values in each plot represent the amplitude of GWs.

B. Strategies for Searching GWs

According to discussed results in previous subsection, we expect that PTR signals detected through our cosmos, to be a proper criterion for detection the footprint of GWs. Randomness of pure PTR s exhibits that any deviation from uncorrelated behavior can be conducted as additional features presented in recorded data. If we can remove other foreground and noises, we are able to conclude that any residual effect may be associated with GWs. On the other hand, referring to theoretical no-

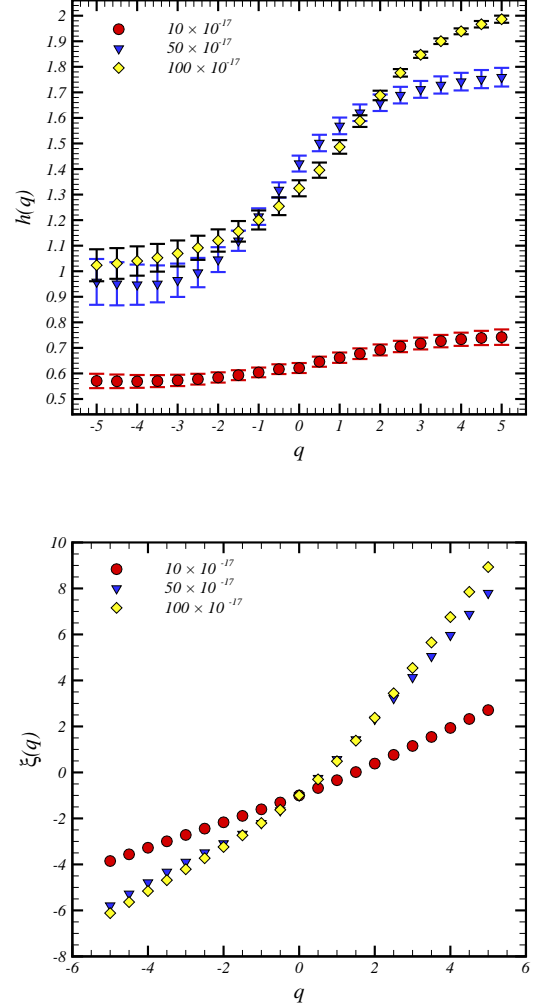


FIG. 6: Upper panel indicates generalized Hurst exponent, $h(q)$, versus q for some PTR s induced by stochastic GWs with $\zeta = -2/3$ calculated by MF-DMA with $\theta = 0.0$. Lower panel illustrates $\xi(q)$ for data sets introduced in upper panel. Different values in each plot represent the amplitude of GWs.

tion for PTR and GWB, we conclude that there exists a potential way for determining the kind of GWs and the value of \mathcal{A} using observed PTR s according to multifractal model. In this section, we are going to introduce robust measures for mentioned purposes.

For detecting global and local GWs, we expect that for GWB (global event) all PTR s signals must be affected by same feature, therefore any global sirens detected in all PTR s refer to probable GWB, while other local events contribute only on some group of PTR s indicating single sources of GWs.

We should notice that any type of GWs can affect on the pure PTR s therefore can be detected by our multifractal analysis. In addition, one can use the following

approaches for determining the value of GWBs amplitude as well. In order to determine the type of stochastic gravitational wave background with strain spectrum modeled by Eq. (26), after preprocessing to remove noise and foreground, we apply multifractal methods to compute reliable Hurst exponent. This exponent has relation to power spectrum exponent as mentioned in table I. Therefore the value of ζ can be determined, conservatively [6]. Since, in real data sets, there are many reasons leading to more complicated inference about the detectability of GWs, in this paper we introduce three criteria as below: I) We showed that Hurst exponent for pure *PTRs* is almost 0.5, while for those signal affected by GWs (Eq. (26)) for a given amplitude, \mathcal{A} and ζ , we get deviation for computed Hurst exponent associated with pure signal. Therefore the measure $\Delta h_1(\mathcal{A}, \zeta) \equiv \sum_{q=q_{min}}^{q_{max}} |h(q) - h_{shuf}(q)|$ can be a good benchmark for quantifying the intensity of GWBs. In this measure $h_{shuf}(q)$ refers to underlying data which is randomized and "shuf" is abbreviation for shuffled. For completely monofractal random series, we have $h_{shuf}(q) = 0.50$. This measure is able to quantify any multifractal nature due to different correlation features existed in different scales of fluctuations in data sets. A systematic way to check the reliability of difference scaling exponent is carried out by P-value. A practical way to find robust mathematical relation between $\Delta h_1(\mathcal{A}, \zeta)$ and \mathcal{A} for any given ζ (or equivalently H), is as follows: we do many simulations for a given value of ζ with different \mathcal{A} 's. Corresponding shuffled series are produced using original series. For shuffled data, generalized Hurst exponents and therefore Δh_1 are computed. Our simulations indicate following fitting function for \mathcal{A} versus Δh_1 for $\zeta = -2/3$:

$$\mathcal{A} = a \exp(b\Delta h_1) + c \exp(d\Delta h_1), \quad (30)$$

here $a = 18.02$, $b = 0.21$, $c = -25.11$ and $d = -0.70$. It turns out that this fitting function is not unique and here we select one of them with high goodness of fit.

II) Since GWs may induce non-gaussianity in *PTR*, it is interesting to take into account $\Delta h_2(\mathcal{A}, \zeta) \equiv \sum_{q=q_{min}}^{q_{max}} |h(q) - h_{sur}(q)|$. In mentioned criterion, $h_{sur}(q)$ is generalized Hurst exponents computed for Gaussian data sets with the same correlation function as original series. Here, "sur" represents surrogated data or phase-randomized surrogated series including the multiplication of Fourier Transform data by a random phase with uniformly distribution function and using inverse Fourier Transform, based on central limit theorem, retrieved data collapses to Gaussian series [102]. We simulated *PTR* accompanying GWBs with different amplitudes and following fitting function is determined for \mathcal{A} as a function of Δh_2 for $\zeta = -2/3$:

$$\mathcal{A} = a\Delta h_2 + b, \quad (31)$$

where $a = 39.67$ and $b = -55.94$.

III) The width of singularity spectrum representing a measure for quantifying the nature of multifractality is

also other benchmark for detecting and determining amplitude of GWs superimposed on *PTRs*. This measure is defined by $\Delta h_3 \equiv |\Delta\alpha - \Delta\alpha_{pure}|$. According to our simulations with ensemble averaging approach, we find:

$$\mathcal{A} = a \exp(b\Delta h_3) + c \exp(d\Delta h_3), \quad (32)$$

for $\zeta = -2/3$. Here $a = 11$, $b = 2.58$, $c = -38.01$ and $d = -4.81$.

Our strategy based on above criteria for searching GWs in observation is generally considered as follows: As explained in section III, In the case of proper value of signal to noise, for each observed *PTR*, we remove all parts related to foreground and other well-known sources, then we apply AD or SVD methods followed by MF-DFA or MF-DMA on clean data to compute $h(q)$ and clarify Hurst exponent. Subsequently the value of ζ is determined. According to each benchmarks, relevant quantities will be computed. For given values of Δh_1 , Δh_2 , Δh_3 , we conservatively read the amplitude of GWs from corresponding figures indicated in Fig. 7 or by relevant equations. It is worth noting that, the functional form for Δh 's should be determined for each value of ζ . Our simulations indicate that, GWs with dimensionless amplitude greater than $\mathcal{A} \geq 10^{-17}$ can be detected according to mentioned benchmarks irrespective to value of ζ .

C. Implementation on Observed Data

Before applying any additional programming to discriminate between trend and fluctuations with high frequency in observed data, we apply DFA and DMA on data. The upper panel of Fig 8 indicates the fluctuation function for $q = 2$ computed by MF-DFA and lower panel illustrates same function just by using MF-DMA methods for various observed *PTRs*. These results confirm that there is a crossover in fluctuation functions versus s . This crossover corresponds to $s_x \sim 60$ days and this crossover is probably associated with instability of atomic time [103]. The scaling exponent for $s < s_x$ is in interval $h(2) \in [1.23, 1.90]$ demonstrating that data sets have non-stationary nature, while for $s > s_x$ we find $h(2) \in [0.25, 1.25]$.

In order to find reliable scaling exponent we apply AD and SVD separately on observed data sets. Then cleaned data will be used as input for MF-DFA and MF-DMA algorithms. In Fig. 9 we illustrate a typical observed *PTR* with thin solid line and trend determined by AD (upper panel) and SVD (lower panel). The corresponding residue between observed data and trend is plotted in bottom of each panel in this figure. Fig. 10 represents the fluctuations function extracted for a typical signal cleaned by AD and SVD and used as input for DFA and DMA. Accordingly, we are able to determine the scaling exponent of underlying data sets. The slope of fluctuation functions for $q = 2$ in reliable scales is $h(q = 2) \in [1.35, 1.85]$ demonstrating all underlying

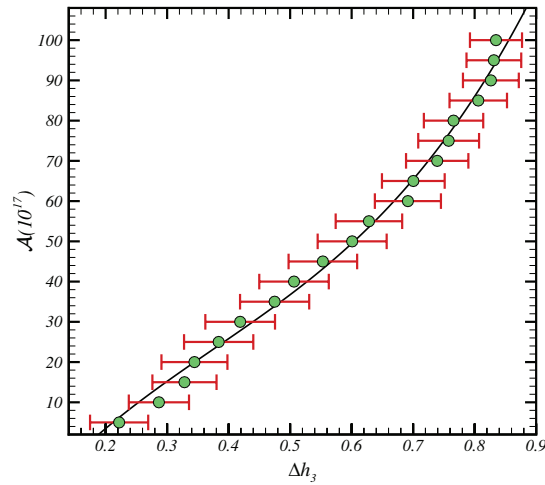
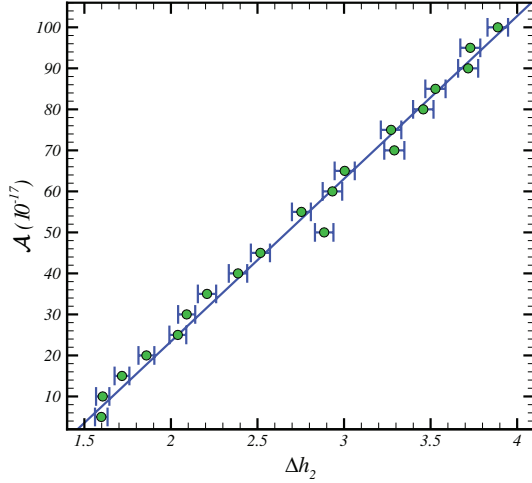
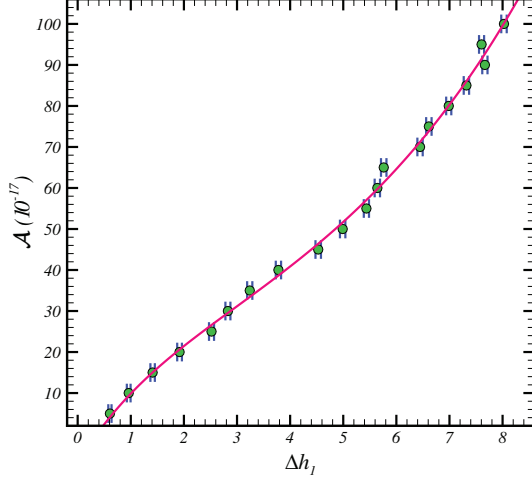


FIG. 7: The value of \mathcal{A} determined by three strategies introduced in this paper only for $\zeta = -2/3$.

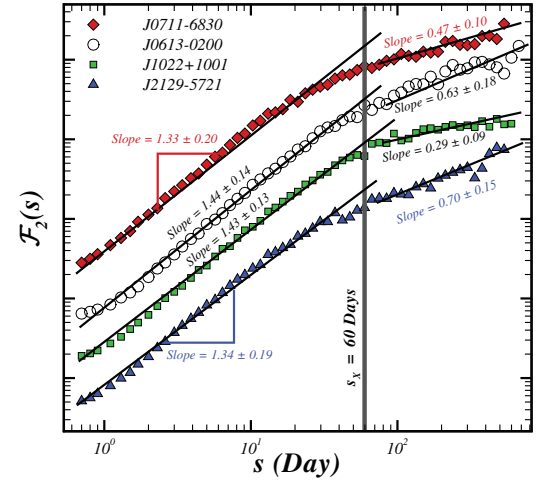
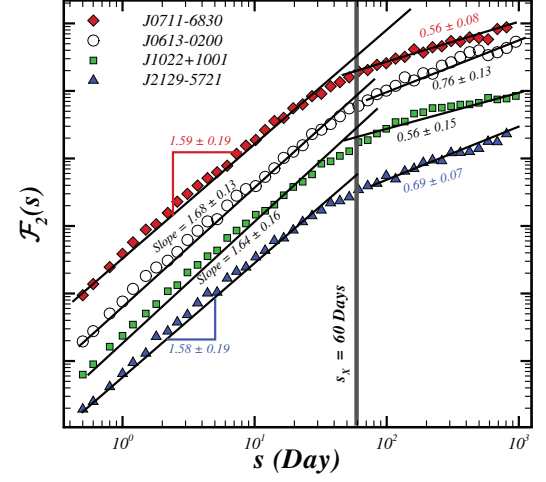


FIG. 8: Upper panel: Log-log plot of $\mathcal{F}_2(s)$ versus s computed according to DFA for various observed data sets. While the lower panel corresponds to same as upper panel computed by backward DMA namely $\theta = 0.0$. To make more sense, we shifted \mathcal{F}_2 vertically for different amplitudes.

series are categorized in non-stationary class. The corresponding Hurst exponent is $H = h(q = 2) - 1$ belonging to $H \in [0.35, 0.85]$. The value of Hurst exponents for all observed PTRs at 68% level of confidence is depicted in Fig. 11. This result confirms that dominant occupation of observed PTRs belongs to long-range correlated behavior. Fig. 12 shows the q -dependency of generalized Hurst exponent after applying SVD on observed data and determined by MF-DMA. The results for MF-DFA are consistent with that of determined by MF-DMA. Since $h(q)$ depends on q , we conclude that all observed PTRs are multifractal. Singularity spectrum of observed PTRs is indicated in Fig. 13. The strength of multifractal-

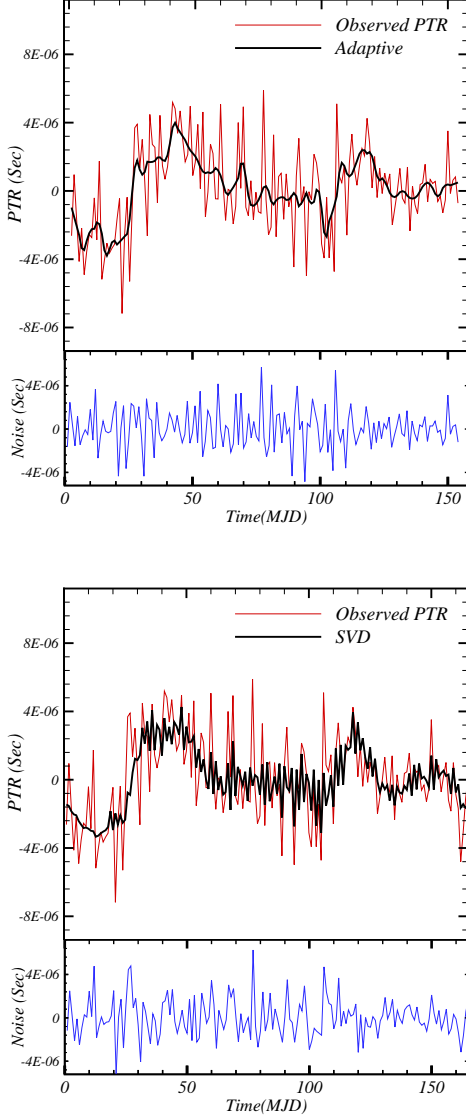


FIG. 9: Implementation of Adaptive method (upper panel) and SVD (lower panel) on PTR of PSR J1603-7202. In each panel top plot corresponds to observed data (thin solid line) and trend (thick solid line), while the bottom represents the residual data corresponding to clean data.

ity nature of PTR s is determined by width of singularity spectrum, $\Delta\alpha = \alpha_{\max} - \alpha_{\min}$. This value for observed data is reported in Tab. II and has been shown in lower panel of Fig. 13. The range of mentioned singularity spectrum is $\Delta\alpha \in [0.90, 3.35]$. Other relevant exponents are reported in Tab. II.

Another interesting question is that: what are the sources of multifractality of observed PTR s? As explained in more details by Kantelhardt et al. [46], in principle, different correlation functions at small and large fluctuations can be considered as a source of multifrac-

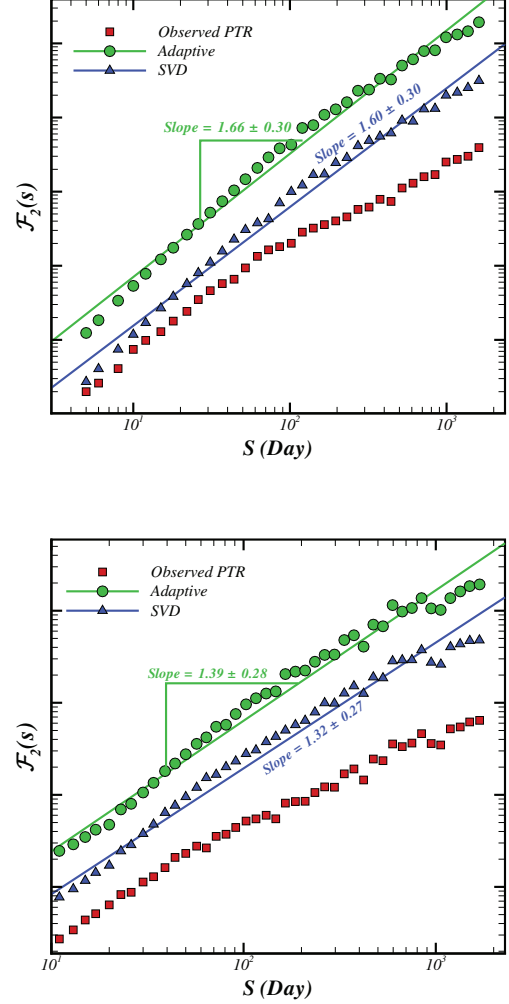


FIG. 10: Log-Log plot of fluctuation function $\mathcal{F}_2(s)$ as a function of s when we apply Adaptive and SVD as pre-processes on PSR J1045-4509. Upper panel is for DFA while lower panel for backward DMA methods. To make more sense, we shifted \mathcal{F}_2 vertically for different series.

tality. Beside mentioned source, heavy-tailed probability distribution contributes in multifractal behavior. In order to distinguish mentioned two types of multifractality, we follow method introduced in [46]. To this end by shuffling series, the scaling behavior of ratio of fluctuation functions $\mathcal{F}_q(s)/\mathcal{F}_q^{\text{shuf}}(s)$ is represented by:

$$\frac{\mathcal{F}_q(s)}{\mathcal{F}_q^{\text{shuf}}(s)} \sim s^{h(q) - h_{\text{shuf}}(q)}, \quad (33)$$

where $h_{\text{shuf}}(q)$ is the generalized hurst exponent of shuffled data. The case $h_{\text{cor}}(q) \equiv h(q) - h_{\text{shuf}}(q) = 0$ refers to multifractality due to distribution function. In this case we can compute $h_{\text{PDF}}(q) \equiv h(q) - h_{\text{sur}}(q)$. If both of $h_{\text{cor}}(q)$ and $h_{\text{PDF}}(q)$ depend on q , two mentioned sources

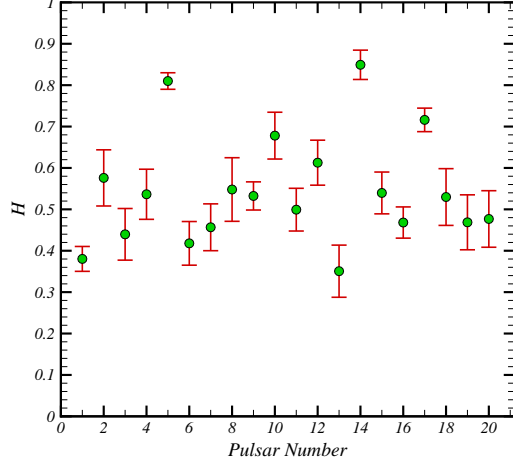


FIG. 11: Hurst exponent of timing residuals of 20 MSPs observed by PPTA.

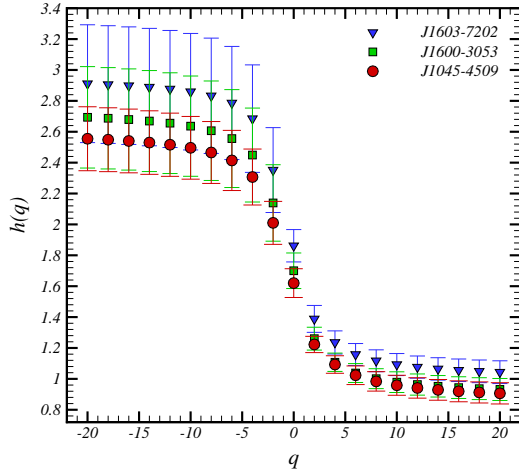


FIG. 12: Generalized Hurst exponent $h(q)$ versus q by SVD-MF-DMA method with $\theta = 0.0$ for some observed timing residuals.

are associated with the nature of multifractality. In our sample, all *PTRs* have $h_{\text{shuf}}(q) = 0.50$ at 1σ confidence interval confirming correlation in data sets is almost the main source of multifractality. This property is a universal feature for all *PTRs* investigated in this paper.

It is worth noting that, for current observational *PTRs*, the scale of imposed fluctuations associated with GWs in *PTRs* is at least one order of magnitude smaller than other sources. Subsequently, based on future generation of surveys including more accurate observational hardware with high value for signal to noise and additional physical information for foreground and other contaminations, various criteria introduced in this paper

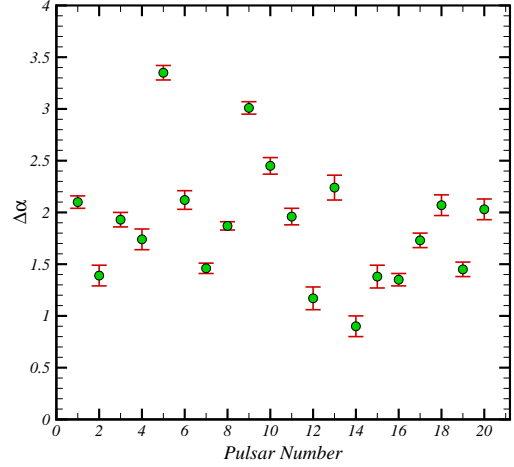
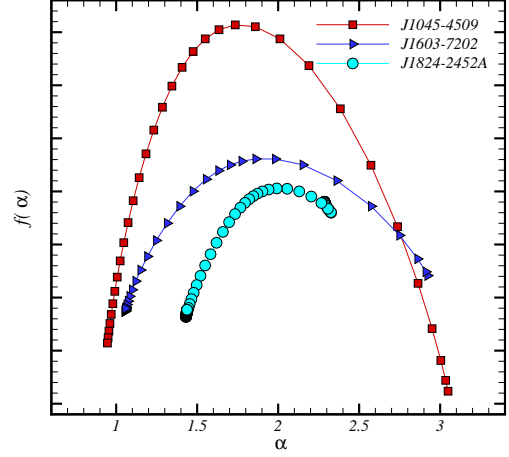


FIG. 13: Upper panel shows the singularity spectrum $f(\alpha)$ versus α for some observed timing residuals. To make more obvious, we shifted $f(\alpha)$ vertically for different series. Lower panel indicates the width of singularity spectrum which is a measure for quantifying multifractality nature of 20 MSPs observed by PPTA.

enable us to detect the footprint of probable GWs.

V. SUMMARY AND CONCLUSION

Pulsar timing residual is a good indicator to examine relevant physical phenomena from interior of pulsars as well as cosmological events superimposed on that. This technique has already caused to abundant important scientific achievements. In spite of high stability in some types of pulsars, superimposed unknown trends and noises cause that mentioned signals to be characterized by stochastic processes. One of the most interesting events to investigate is gravitational wave produced by

TABLE II: Hurst exponent (H) calculated by MF-DFA, rms and total time span (TTS) of post-fit timing residuals of 20 MSPs observed in PPTA project. The error-bar corresponds to 1σ confidence interval.

PSR Number	PSR name	H	$\Delta\alpha$	γ	β	rms (μs)	TTS (years)
1	J0437-4715	0.38 ± 0.03	2.10 ± 0.06	-0.76 ± 0.06	1.76 ± 0.06	0.08	4.76
2	J0613-0200	0.58 ± 0.07	1.39 ± 0.10	-1.15 ± 0.14	2.15 ± 0.14	1.07	5.99
3	J0711-6830	0.44 ± 0.06	1.93 ± 0.07	-0.88 ± 0.12	1.88 ± 0.12	0.89	5.99
4	J1022+1001	0.54 ± 0.06	1.74 ± 0.10	-1.07 ± 0.12	2.07 ± 0.12	1.72	5.88
5	J1024-0719	0.81 ± 0.02	3.35 ± 0.07	-1.62 ± 0.04	2.62 ± 0.04	1.13	5.99
6	J1045-4509	0.42 ± 0.05	2.12 ± 0.09	-0.84 ± 0.11	1.84 ± 0.11	2.77	5.94
7	J1600-3053	0.46 ± 0.06	1.46 ± 0.05	-0.91 ± 0.15	1.91 ± 0.15	0.68	5.93
8	J1603-7202	0.55 ± 0.08	1.87 ± 0.04	-1.10 ± 0.07	2.10 ± 0.07	2.14	5.99
9	J1643-1224	0.53 ± 0.03	3.01 ± 0.06	-1.06 ± 0.11	2.06 ± 0.11	1.64	5.87
10	J1713+0747	0.68 ± 0.06	2.45 ± 0.08	-1.36 ± 0.10	2.36 ± 0.10	0.31	5.71
11	J1730-2304	0.50 ± 0.05	1.96 ± 0.08	-1.00 ± 0.13	2.00 ± 0.13	1.47	5.93
12	J1732-5049	0.61 ± 0.05	1.17 ± 0.11	-1.23 ± 0.07	2.23 ± 0.07	2.22	5.08
13	J1744-1134	0.35 ± 0.06	2.24 ± 0.12	-0.70 ± 0.10	1.70 ± 0.10	0.32	5.87
14	J1824-2452A	0.85 ± 0.04	0.90 ± 0.10	-1.70 ± 0.08	2.70 ± 0.08	2.44	5.75
15	J1857+0943	0.54 ± 0.05	1.38 ± 0.11	-1.08 ± 0.06	2.08 ± 0.06	0.84	5.93
16	J1909-3744	0.47 ± 0.04	1.35 ± 0.06	-0.94 ± 0.13	1.94 ± 0.13	0.13	5.75
17	J1939+2134	0.72 ± 0.03	1.73 ± 0.07	-1.43 ± 0.14	2.43 ± 0.14	0.68	5.88
18	J2124-3358	0.53 ± 0.07	2.07 ± 0.10	-1.06 ± 0.00	2.06 ± 0.00	1.90	5.99
19	J2129-5721	0.47 ± 0.07	1.45 ± 0.07	-0.94 ± 0.00	1.94 ± 0.00	0.80	5.86
20	J2145-0750	0.48 ± 0.07	2.03 ± 0.10	-0.95 ± 0.00	1.95 ± 0.00	0.78	5.99

either primordial or late events. Several pulsar timing arrays have been proposed for this purpose. Quantifying the fluctuations of $PTRs$, can be a proper measure for detecting the benchmark of GWs. In this paper, for the first time, we utilized multifractal approach in order to examine the statistical properties of synthetic and observed $PTRs$ affected by trends and noises. In the presence of trends and unknown noises, only robust methods are able to recover correct multifractal nature of underlying series. In this research, we used MF-DFA and MF-DMA modified by pre-processes so-called AD and SVD algorithms. To check the viability of mentioned methods, we used synthetic data set simulated by TEMPO2 pulsar timing package. A template proposed in [6] has been used for adopting the contribution of GWs. We simulated 100 synthetic $PTRs$ and they have been used as inputs for MF-DFA and MF-DMA methods. Our results demonstrated that the ensemble average of Hurst exponent of simulated data is $\langle H \rangle = 0.51 \pm 0.02$ confirming pure $PTRs$ belong to monofractal uncorrelated stationary process. There is no crossover in fluctuation functions versus scale determined by MF-DFA and MF-DMA (Fig. 3). Adding mock GWB signal on pure $PTRs$ leads to have crossover in log-log plot of \mathcal{F}_2 as a function of s as indicated in Fig. 5. In order to make a decision regarding the scaling behavior of $PTRs$ induced by GWs, we carried out SVD and AD methods on data. We found that, SVD can remove the crossover on fluctuation function for any q . Therefore, we were able to

classify mentioned data in universal class of multifractal process. The time scale for crossover depends on intensity of GWs signal and the method that is implemented for analysis. In the presence of GWs, $PTRs$ belong to multifractal process due to q -dependency of generalized Hurst exponent ($h(q)$) (see Fig. 6).

The value of multifractality is grown up by increasing the intensity of GWs, subsequently, this provided this idea that the nature of multifractality beside other changing in behavior of $\mathcal{F}_2(s)$ can potentially be an indicator of GWs. To ensure that, we conservatively consider all effects as much as possible. We proposed three criteria to quantify the footprint of GWs on pulsar timing residuals. First approach corresponds to comparing $h(q)$ with that of computed for shuffled series. Comparison between $h(q)$ and generalized Hurst exponent computed for Gaussian signal is second criterion. As stated before, adding GWs on $PTRs$, the nature of multifractality becomes obvious, therefore a relevant quantity for quantify this behavior is width of singularity spectrum, namely $\Delta\alpha$. Consequently, the width of singularity spectrum can be used for third approach. Accordingly, the strategy for GWs detection in observation is as follows: After removing all effects of foreground and systematic noises, we must apply SVD or AD on datasets and cleaned data will be used as input for MF-DFA or MF-DMA methods. The type of superimposed GWs can be recognized by determining Hurst exponent. Finally, the dimensionless amplitude of expected GWs (\mathcal{A}) can be determined

by inserting relevant quantities extracted by mentioned analyses in Eqs. (30), (31) and (32). For a stochastic gravitational wave background with characteristic strain spectrum described by $\mathcal{H}_c(f) \sim \mathcal{A}f^\zeta$, the dimensionless amplitude greater than $\mathcal{A} \gtrsim 10^{-17}$ can be recognized irrespective to value of ζ .

For the last part of this study, we considered MSPs observed by PPTA project. We found that a crossover at $s_\times \sim 60$ days for all observed pulsars used in this paper. Instability of atomic time for mentioned observations is a candidate for the reason of this systematic crossover. The intervals of generalized Hurst exponent for $q = 2$ for $s < s_\times$ and $s > s_\times$ are $h(2) \in [1.23, 1.90]$ and $h(2) \in [0.25, 1.25]$, respectively. After applying SVD, corresponding Hurst exponent belongs $H \in [0.35, 0.85]$ indicated in Fig. 11. The q -dependency of $h(q)$ confirmed that all observed MSPs behave as multifractal field. The rest of relevant exponents for observed MSPs has been reported in Tab. II. The source of multifractality is almost supported by correlation in small and large scales and becomes a universal property of all observed pulsars examined in this paper. In order to use current available MSPs to detect GWs, an important challenge is the

availability of high precision pulsar timing experiment as well as computation of more accurate arrival time. As depicted in Figs. 1 and 2, the usage of current available MSPs encounters with some difficulties due to low value of signal to noise and other technical problems related to measurements, therefore, in the next generation of experiments, the opportunity for searching GWs via pulsar timing residuals will be achieved practically. It could be interesting to simulate various kinds of GWs and accomplish with *timing noise* to check the robustness of proposed method in this research. Sensitivity to frequency is beyond the scope of this paper and it must be done elsewhere.

VI. ACKNOWLEDGMENT

The authors thank Reza Monadi for his useful discussion. SMSM is grateful to school of Physics, Institute for research in fundamental sciences (IPM), where some parts of this paper have been finalized there.

-
- [1] Verbiest, J. P. W., Lentati, L., Hobbs, G., van Haasteren, R., Demorest, P. B., Janssen, G. H., ... & Champion, D. J. 2016, Monthly Notices of the Royal Astronomical Society, 458(2), 1267-1288.
 - [2] Lorimer, D. R., & Kramer, M. 2005, Handbook of pulsar astronomy (Vol. 4). Cambridge University Press.
 - [3] Manchester, R. N., Hobbs, G., Bailes, M., Coles, W. A., van Straten, W., Keith, M. J., ... & You, X. P. 2013, Publications of the Astronomical Society of Australia, 30, e017.
 - [4] Sazhin M. V., 1978, SvA, 22, 36.
 - [5] Detweiler S., 1979, ApJ, 234, 1100.
 - [6] Hobbs, G., Jenet, F., Lee, K. J., Verbiest, J. P. W., Yardley, D., Manchester, R., ... & Shettigara, C. 2009, Monthly Notices of the Royal Astronomical Society, 394(4), 1945-1955.
 - [7] Peters P. C. 1964, Phys. Rev. , 136, 1224.
 - [8] Thorne K. S., & Braginskii V. B. 1976, ApJ, 204, L1.
 - [9] Damour T., & Vilenkin A. 2001, Phys. Rev. , 64(6), 064008.
 - [10] Kocsis B., Gáspár M. E., & Marka S. 2006, ApJ, 648, 411.
 - [11] Enoki M., Nagashima M. 2007, Progress of Theoretical Physics, 117, 241.
 - [12] Maggiore, M. 2000, gravitational wave experiments and early universe cosmology. Phys. Rep. 331, 283-367
 - [13] Hobbs, G. 2011. In High-Energy Emission from Pulsars and their Systems (pp. 229-245), Springer Berlin Heidelberg.
 - [14] Damour, T., & Vilenkin, A. 2005. Physical Review D, 71(6), 063510.
 - [15] Pshirkov, M. S., & Tuntsov, A. V. 2010, Physical Review D, 81(8), 083519.
 - [16] Rajagopal, M., Romani, R. W. 1995, ApJ 446, 543549
 - [17] Taylor, S. R., & Gair, J. R. 2012, Physical Review D, 86(2), 023502.
 - [18] Mandic, V., Bird, S., & Cholis, I. 2016, arXiv preprint arXiv:1608.06699.
 - [19] Meadors, G. D. 2014, Directed searches for continuous gravitational waves from spinning neutron stars in binary systems (Doctoral dissertation, The University of Michigan).
 - [20] Coyne, R., Corsi, A., & Owen, B. J. 2016, Physical Review D, 93(10), 104059.
 - [21] Pai, A., Dhurandhar, S., & Bose, S. 2001, Physical Review D, 64(4), 042004.
 - [22] Zhu, X. J., Hobbs, G., Wen, L., Coles, W. A., Wang, J. B., Shannon, R. M., ... & Dai, S. 2014, Monthly Notices of the Royal Astronomical Society, 444(4), 3709-3720.
 - [23] Jenet, F. A., Hobbs, G. B., Lee, K. J., & Manchester, R. N. 2005, The Astrophysical Journal Letters, 625(2), L123.
 - [24] Taylor Jr, J. H. 1994, Binary pulsars and relativistic gravity. Reviews of Modern Physics, 66(3), 711.
 - [25] Roebber, E., & Holder, G. 2016, arXiv preprint arXiv:1609.06758.
 - [26] Jenet, F. A., Hobbs, G. B., van Straten, W., Manchester, R. N., Bailes, M., Verbiest, J. P. W., ... & Ord, S. M. 2006, The Astrophysical Journal, 653(2), 1571.
 - [27] Manchester, R. N. 2008, AIP, Conference Proceedings, Volume 983, 584
 - [28] Hobbs, G. 2013, Classical and Quantum Gravity, 30(22), 224007.
 - [29] Janssen, G. H. et al. 2008, AIP, Conference Proceedings, Volume 983, 633
 - [30] Kramer, M., & Champion, D. J. 2013, Classical and Quantum Gravity, 30(22), 224009.

- [31] Demorest, P., Lazio, J., & Lommen, A. 2009, arXiv preprint arXiv:0902.2968.
- [32] McLaughlin, M. A. 2013, *Classical and Quantum Gravity*, 30(22), 224008.
- [33] Cordes, J. M., Kramer, M., Lazio, T. J. W., Stappers, B. W., Backer, D. C., & Johnston, S. 2004, *New Astronomy Reviews*, 48(11), 1413-1438.
- [34] Lazio, T. J. W. 2013, *Classical and Quantum Gravity*, 30(22), 224011.
- [35] Zhu, X. J., Wen, L., Hobbs, G., Zhang, Y., Wang, Y., Madison, D. R., ... & Wang, J. B. 2015, *Monthly Notices of the Royal Astronomical Society*, 449(2), 1650-1663.
- [36] Zhu, X. J., Wen, L., Xiong, J., Xu, Y., Wang, Y., Mohanty, S. D., ... & Manchester, R. N. 2016, *Monthly Notices of the Royal Astronomical Society*, 461(2), 1317-1327.
- [37] Lommen, A. N. 2015, *Reports on Progress in Physics*, 78(12), 124901.
- [38] Ellis, J. 2014, *Searching for Gravitational Waves Using Pulsar Timing Arrays* PhD thesis, The University of Wisconsin-Milwaukee.
- [39] R. N. Manchester, arXiv:1004.3602
- [40] Hellings, R. W., & Downs, G. S. 1983, *The Astrophysical Journal*, 265, pp.L39-L42.
- [41] Hurst, H. E. 1951, *Trans. Amer. Soc. Civil Eng.*, 116, 770-808.
- [42] Tessier, Y., Lovejoy, S., Hubert, P., Schertzer, D., & Pecknold, S. 1996, *Journal of Geophysical Research: Atmospheres*, 101(D21), 26427-26440.
- [43] Pandey, G., Lovejoy, S., & Schertzer, D. 1998, *Journal of Hydrology*, 208(1), 62-81.
- [44] Pelletier, J. D., & Turcotte, D. L. 1997, *Journal of Hydrology*, 203(1), 198-208.
- [45] Peng, C. K., Havlin, S., Stanley, H. E., & Goldberger, A. L. 1995, *Chaos: An Interdisciplinary Journal of Nonlinear Science*, 5(1), 82-87.
- [46] Kantelhardt, J. W., Zschiegner, S. A., Koscielny-Bunde, E., Havlin, S., Bunde, A., & Stanley, H. E. 2002, *Physica A: Statistical Mechanics and its Applications*, 316(1), 87-114.
- [47] Gu, G. F., & Zhou, W. X., 2010, *Physical Review E*, 82(1), 011136.
- [48] Shao, Y. H., Gu, G. F., Jiang, Z. Q., & Zhou, W. X., 2015, *Fractals*, 23(03), 1550034.
- [49] Hobbs, G. B., Edwards, R. T., & Manchester, R. N. 2006, *Monthly Notices of the Royal Astronomical Society*, 369(2), 655-672.
- [50] Hu, J., Gao, J., & Wang, X. 2009, *Journal of Statistical Mechanics: Theory and Experiment*, 2009(02), P02066.
- [51] Golub, G., Van Loan, C. 1996, *The Johns Hopkins University Press Ltd.*, London.
- [52] Nagarajan, R., & Kavasseri, R. G. 2005, *Chaos, Solitons & Fractals*, 26(3), 777-784.
- [53] Nagarajan, R., & Kavasseri, R. G. 2005, *Physica A: Statistical Mechanics and its Applications*, 354, 182-198.
- [54] Wu, Z., Huang, N. E., Long, S. R., & Peng, C. K. 2007, *Proceedings of the National Academy of Sciences*, 104(38), 14889-14894.
- [55] Mantegna, R. N., & Stanley, H. E. 2000, *Cambridge, UK: Cambridge University.*
- [56] Liu, Y., Gopikrishnan, P., & Stanley, H. E. 1999, *Physical review e*, 60(2), 1390.
- [57] Vandewalle, N., Ausloos, M., & Boveroux, P. 1999, *Physica A: Statistical Mechanics and its Applications*, 269(1), 170-176.
- [58] Ivanov, P. C., Yuen, A., Podobnik, B., & Lee, Y. 2004, *Physical Review E*, 69(5), 056107.
- [59] Movahed, M. S., & Hermanis, E. 2008, *Physica A: Statistical Mechanics and its Applications*, 387(4), 915-932.
- [60] Movahed, M. S., Jafari, G. R., Ghasemi, F., Rahvar, S., & Tabar, M. R. R. 2006, *Journal of Statistical Mechanics: Theory and Experiment*, 2006(02), P02003.
- [61] Movahed, M. S., Ghasemi, F., Rahvar, S., & Tabar, M. R. R. 2011, *Physical Review E*, 84(2), 021103.
- [62] Jafari, G. R., Pedram, P., & Hedayatifar, L. 2007, *Journal of Statistical Mechanics: Theory and Experiment*, 2007(04), P04012.
- [63] Jennings, H. D., Ivanov, P. C., Martins, A. D. M., da Silva, P. C., & Viswanathan, G. M. 2004, *Physica A: Statistical Mechanics and its Applications*, 336(3), 585-594.
- [64] Kimiagar, S., Movahed, M. S., Khorram, S., Sobhanian, S., & Tabar, M. R. R. 2009, *Journal of Statistical Mechanics: Theory and Experiment*, 2009(03), P03020.
- [65] Xiao-Yan, Z., Zong-Hua, L., & Ming, T., *J. Stat.* 2007, *Chinese Physics Letters*, 24(7), 2142.
- [66] Soares, F., Freire, M. M., Pereira, M., Janela, F., & Seabra, J. 2009, In 2009 IEEE Pacific Rim Conference on Communications, Computers and Signal Processing (pp. 677-681). IEEE.
- [67] Soares, F., Sousa, I., Janela, F., Seabra, J., Pereira, M., & Freire, M. M. 2010, In *Medical Measurements and Applications Proceedings (MeMeA)*, 2010 IEEE International Workshop on (pp. 161-164). IEEE.
- [68] Zunino, L., Gulich, D., Funes, G., & Ziad, A. 2014, *Optics letters*, 39(13), 3718-3721. 1390 (1999).
- [69] Podobnik, B., & Stanley, H. E. 2008, *Physical review letters*, 100(8), 084102.
- [70] Podobnik, B., Grosse, I., Horvatic, D., Ilic, S., Ivanov, P. Ch., and Stanley, H. E. 2009, *Eur. Phys. J. B* 71, 243-250,
- [71] Podobnik, B., Jiang, Z. Q., Zhou, W. X. and Stanley, H. E. 2011, *Physical Review E* 84, 066118.
- [72] Qian, X. Y., Liu, Y. M., Jiang, Z. Q. and Podobnik, B., Zhou, W. X., Stanley, H. E. 2015, *Phys. Rev. E* 91, 062816.
- [73] Zebende G. F., *Physica A* 390 (2011) 614?618
- [74] Zebende, G. F., da Silva, M. F., Filho A. M., *Physica A* 392 (2013) 1756?1761.
- [75] Zhou, W. X. 2008, *Physical Review E*, 77(6), 066211.
- [76] Hu, K., Ivanov, P. C., Chen, Z., Carpena, P., & Stanley, H. E. 2001, *Physical Review E*, 64(1), 011114.
- [77] Chen, Z., Ivanov, P. C., Hu, K., & Stanley, H. E. 2002, *Physical Review E*, 65(4), 041107.
- [78] Chianca, C. V., Ticona, A., & Penna, T. J. P. 2005, *Physica A: Statistical Mechanics and its Applications*, 357(3), 447-454.
- [79] Nagarajan, R., & Kavasseri, R. G. 2005, *International Journal of Bifurcation and Chaos*, vol.15, no.2, 1767-1773 (2005).
- [80] Huang, N. E., Shen, Z., Long, S. R., Wu, M. C., Shih, H. H., Zheng, Q., ... & Liu, H. H. 1998. In *Proceedings of the Royal Society of London A: Mathematical, Physical and Engineering Sciences* (Vol. 454, No. 1971, pp. 903-995). The Royal Society.
- [81] Peng, C. K., Buldyrev, S. V., Goldberger, A. L., Havlin, S., Sciortino, F., Simons, M., & Stanley, H. E. 1992, *Nature*, 356(6365), 168-170.

- [82] Peng, C. K., Buldyrev, S. V., Havlin, S., Simons, M., Stanley, H. E., & Goldberger, A. L. 1994, Mosaic organization of DNA nucleotides. *Physical review e*, 49(2), 1685.
- [83] Shao, Y. H., Gu, G. F., Jiang, Z. Q., Zhou, W. X., & Sornette, D. 2012, *Scientific reports*, 2.
- [84] Buldyrev, S. V., Goldberger, A. L., Havlin, S., Mantegna, R. N., Matsu, M. E., Peng, C. K., ... & Stanley, H. E. 1995, *Physical Review E*, 51(5), 5084.
- [85] Bunde, A., Havlin, S., Kantelhardt, J. W., Penzel, T., Peter, J. H., & Voigt, K. 2000, *Physical Review Letters*, 85(17), 3736.
- [86] Taqqu, M. S., Teverovsky, V., & Willinger, W. 1995, *Fractals*, 3(04), 785-798.
- [87] Ossadnik, S. M., Buldyrev, S. V., Goldberger, A. L., Havlin, S., Mantegna, R. N., Peng, C. K., ... & Stanley, H. E. 1994, *Biophysical Journal*, 67(1), 64.
- [88] Halsey, T. C., Jensen, M. H., Kadanoff, L. P., Procaccia, I., & Shraiman, B. I. 1986, *Physical Review A*, 33(2), 1141.
- [89] Feder, J. 1989, Springer Science + Business Media, LLC.
- [90] Muzy, J. F., Bacry, E., & Arneodo, A. 1994, *International Journal of Bifurcation and Chaos*, 4(02), 245-302.
- [91] Arneodo, A., Bacry, E., & Muzy, J. F. 1995, *Physica A: Statistical Mechanics and its Applications*, 213(1), 232-275.
- [92] Xu, L., Ivanov, P. C., Hu, K., Chen, Z., Carbone, A., & Stanley, H. E. 2005, *Physical Review E*, 71(5), 051101.
- [93] Kantelhardt, J. W., Koscielny-Bunde, E., Rego, H. H., Havlin, S., & Bunde, A. 2001, *Physica A: Statistical Mechanics and its Applications*, 295(3), 441-454.
- [94] Hajian, S., & Movahed, M. S., 2010, *Physica A: Statistical Mechanics and its Applications*, 389(21), 4942-4957.
- [95] Shang, P., Lin, A., & Liu, L. 2009, *Physica A: Statistical Mechanics and its Applications*, 388(5), 720-726.
- [96] Colistete Jr, R., Fabris, J. C., Goncalves, S. V. B., & De Souza, P. E. 2004, *International Journal of Modern Physics D*, 13(04), 669-693.
- [97] Yardley, D. R. B. 2011, University of Sydney.
- [98] Sesana, A., Vecchio, A., & Colacino, C. N. 2008, *Monthly Notices of the Royal Astronomical Society*, 390(1), 192-209.
- [99] Taylor, S. R., & Gair, J. R. 2013, *Physical Review D*, 88(8), 084001.
- [100] <http://www.atnf.csiro.au/research/pulsar/ppta/>
- [101] Edwards, R. T., Hobbs, G. B., & Manchester, R. N. 2006, *Monthly Notices of the Royal Astronomical Society*, 372(4), 1549-1574.
- [102] Prichard D. and Theiler J. 1994, *Phys. Rev. Lett.* 73, 951.
- [103] Petit, G. 1995, Limits to the stability of pulsar time. BUREAU INTERNATIONAL DES POIDS ET MESURES SEVRES (FRANCE).